Published in final edited form as:
Acta Biomater. 2011 January ; 7(1): 268–277. doi:10.1016/j.actbio.2010.07.036.

Immobilization of a phosphonated analog of matrix phosphoproteins within cross-linked collagen as a templating mechanism for biomimetic mineralization

Li-sha Gu[1], **Young Kyung Kim**[2], **Yan Liu**[3], **Kei Takahashi**[4], **Senthil Arun**[5], **Courtney E. Wimmer**[6], **Raquel Osorio**[7], **Jun-qi Ling**[1,*], **Stephen W. Looney**[6], **David H. Pashley**[8], and **Franklin R. Tay**[8,9,*]

[1] Department of Operative Dentistry and Endodontics, Guanghua School of Stomatology, Sun Yat-sen University, 56 Lingyuanxi Road, Guangzhou, China

[2] Department of Conservative Dentistry, School of Dentistry, Kyungpook National University, 2-188-1, Samduk-dong, Jung-gu, Daegu, Korea

[3] Department of Stomatology, Tongji Hospital, Huazhong University of Science and Technology, 1095 Jiefang Rd., Wuhan, China

[4] Department of Operative Dentistry, Okayama University, Okayama, Japan

[5] Department of Preventive and Restorative Sciences, School of Dental Medicine, University of Pennsylvania, Philadelphia, PA

[6] Department of Biostatistics, Medical College of Georgia, 1120 15th street, Augusta, Georgia, USA

[7] Department of Dental Materials. School of Dentistry, University of Granada, Av. de Madrid s/n, Granada, Spain

[8] Department of Oral Biology, School of Dentistry, Medical College of Georgia, 1120 15th street, Augusta, GA, USA

[9] Department of Endodontics, School of Dentistry, Medical College of Georgia, 1120 15th street, Augusta, GA, USA

Abstract

Immobilization of phosphoproteins on a collagen matrix is important for induction of intrafibrillar apatite mineralization. Unlike phosphate esters, polyphosphonic acid has no reactive sites for covalent binding to collagen amine groups. Binding of polyvinylphosphonic acid (PVPA), a biomimetic templating analog of matrix phosphoproteins, to collagen was found to be electrostatic in nature. Thus, an alternative retention mechanism was designed for immobilization of PVPA to collagen by cross-linking the latter with carbodiimide (EDC). This mechanism is based on the principle of size exclusion entrapment of PVPA molecules within the internal water compartments of collagen. By cross-linking collagen with EDC, a zero-length cross-linking agent, the sieving property of collagen is increased, enabling the PVPA to be immobilized within the collagen. Absence of covalent cross-linking between PVPA and collagen was confirmed by FT-IR spectroscopy. Based

[*]Co-Corresponding Authors: Dr. Franklin Tay - Tel.: +1 706 721 2033; Fax: +1 706 721 6252; ftay@mcg.edu. Dr. Jun-qi Ling (supervisor of first author's PhD dissertation in China) - Tel: +8620-83862558; Fax: +8620-83870412; lingjq@mail.sysu.edu.cn.

on these results, a concentration range for immobilized PVPA to template intrafibrillar apatite deposition was established and validated using a single-layer reconstituted type I collagen mineralization model. In the presence of a polyacrylic acid-containing mineralization medium, optimal intrafibrillar mineralization of the EDC-cross-linked collagen was achieved using 500 and 1,000 μg/mL PVPA. The mineralized fibrils exhibited a hierarchical order of intrafibrillar mineral infiltration, as manifested by the appearance of electron-dense periodicity within unstained fibrils. Understanding the basic processes in intrafibrillar mineralization of reconstituted collagen creates opportunities for the design of tissue engineering materials for hard tissue repair and regeneration.

Keywords

cross-linking; intrafibrillar mineralization; reconstituted collagen; size exclusion; templating analog

1. Introduction

Type I collagen serves as scaffolds for biomineralization of bone and dentin. In the absence of apatite seed crystallites, a collagen matrix alone does not possess the thermodynamic and kinetic mechanisms for induction of apatite nucleation [1]. There is considerable evidence supporting that intrafibrillar mineralization of collagen is regulated by two concerted processes in biomineralization. The first is the sequestration of amorphous mineral phases into nanoprecursors that control the ultimate dimensions of the deposited minerals [2]. The second is the templating of mineral nucleation along specific sites (gap zones) of the collagen fibril to control the hierarchy of crystallite arrangement. Both processes are mediated by noncollagenous matrix proteins (NCPs), a group of acidic, carboxylic acid and/or phosphate-containing proteins that are essential for regulation of tissue mineralization [3,4]. Until now, the therapeutic use of native or recombinant NCPs as nucleating agent for *in-situ* biomineralization is not yet economically viable. Accordingly, scientists have resorted to the use of poly(anionic) acid molecules to mimic the functional domains of naturally occurring proteins [5].

Based on the aforementioned two-step motif, a nanotechnology-inspired [6] design for biomimetic mineralization of demineralized dentin collagen has been reported with the use of two poly(anionic) analogs of NCPs [7,8]. One biomimetic analog is a low molecular weight carboxylated polyelectrolyte which is used to sequester metastable amorphous mineral nanoprecursors derived from solutions via a liquid-liquid phase separation mechanism [9,10]. The fluid-like mineral nanoprecursor droplets infiltrate collagen fibrils by capillary action to fill the gap zones between the collagen molecules and spaces between the microfibrils [11]. This non-classical crystallization approach is based on the use of a polymer-induced liquid-precursor phase [9,11] and differs from the classical view of how apatite crystallites are nucleated from ions within the gap zones, and subsequently grow to produce mineralized biocomposites [12]. Nevertheless, it is compatible with the observation of amorphous mineral phases in biomineralization systems [13,14]. The other phosphonated polyelectrolyte mimics the mineral induction function of immobilized matrix phosphoproteins to collagen [15]. It has been shown that phosphoproteins are non-specific and may be substituted by other immobilized, naturally-occurring phosphoproteins to induce apatite deposition within collagen [16,17]. When bound to collagen, the phosphonated polyelectrolyte is conjectured to perform a similar templating function by guiding the nucleation and spatial orientation of mesocrystalline apatite phases from the infiltrated mineral nanoprecursors and to induce their self-assembly into nanocrystals [6,18,19]. As this process occurs within and along collagen fibrils, this results in intrafibrillar and interfibrillar mineralization of the fibrils.

In our proof-of-concept design [7,8], both the sequestration and templating analogs are dissolved in simulated body fluid (SBF) and rely on diffusion to reach the collagen matrix. For *in-situ* translation of this technology to regenerative medicine and dentistry, it is not desirable to rely on this strategy for delivery of the templating biomimetic analog. Matrix phosphoproteins involved in biomineralization are complexed to different locations along the collagen molecule [15]. Their immobilization on the collagen matrix via covalent cross-linking is crucial for induction of intrafibrillar mineralization [20,21]. Thus, it is logical to examine the feasibility of doping type I collagen with polyvinylphosphonic acid (PVPA), a phosphonated templating analog of matrix phosphoproteins, as the part of our translational strategy. Unlike phosphate esters (C-O-P), polyphosphonic acid (C-P) has no reactive sites for covalent binding to collagen amine groups [22]. Thus, PVPA binding to collagen is likely to be electrostatic in nature [23] and may desorb from the collagen matrix after exposure to water or interstitial fluids. This necessitates the development of an alternative mechanism for immobilizing PVPA within collagen.

Water-soluble 1-ethyl-3-(3-dimethylaminopropyl)-carbodiimide (EDC) is a biocompatible, zero-length cross-linking agent that catalyzes the formation of amide bonds between carboxyl/phosphate and amine groups via the formation of O-acylisourea derivatives. It induces direct linking of two chemical groups without incorporating extrinsic spacers between the cross-linked moieties [24]. N-hydroxysuccinimide (NHS) is frequently used to increase the efficiency of EDC-mediated coupling reactions [25]. Coupling of the 5′ terminal phosphate nucleotides to amine-containing molecules may also be achieved using EDC and imidazole (Im) via the formation of phosphorylimidazole intermediates [26]. We hypothesize that cross-linking of collagen via the use of a zero-length cross-linking agent will augment the size exclusion effect of collagen fibrils [27], enabling PVPA molecules to be trapped within the collagen internal water compartments during biomimetic mineralization. This will allow us to remove this templating analog from the mineralization medium.

The objectives of this study were to examine the binding characteristics of PVPA to demineralized dentin collagen, to determine whether immobilization of PVPA to collagen matrices and intrafibrillar mineralization of the collagen could be achieved by cross-linking collagen with different EDC-mediated strategies. The null hypotheses tested were: (1) Binding of PVPA to demineralized collagen matrices is not affected by the time employed for binding, (2) There is no difference in the stability of PVPA immobilization irrespective of whether collagen is cross-linked by EDC, and (3) There is no advantage in using NHS or IM with EDC for cross-linking collagen to immobilize PVPA within demineralized collagen matrices. A PVPA immobilization protocol was selected based on these criteria for evaluating the effect of PVPA concentrations on intrafibrillar mineralization of reconstituted type I collagen fibrils.

2. Materials and methods

2.1 Preparation of demineralized collagen matrices

Five hundred extracted human third molars were obtained with patient informed consent under a protocol approved by the Human Assurance Committee of the Medical College of Georgia. Radicular dentin ground free of enamel, cementum and pulpal soft tissues was reduced to a fine powder by freezing the dentin pieces in liquid nitrogen and triturating them in a stainless steel mixer mill (Model MM301, Retsch, Newtown, PA) for 10 min at 30 Hz. The powder was mechanically sieved to a particle size smaller than 38 μm, with all particles below this cutoff dimension retained. Aliquots of dentin powder were immersed for 48 h in 4M guanidine HCl buffered to pH 7.4 with 0.05 M Tris HCl for initial dissociative extraction of NCPs They were then completely demineralized in 0.5 M ethylenediamine tetraacetic acid at 4 °C. Absence of residual minerals was confirmed using digital radiography. Thereafter, the demineralized dentin aliquots were treated with 4 M guanidine HCl containing protease inhibitors for 48 h at

4 °C for extraction of the tightly bound NCPs that were previously masked by minerals [28]. All solutions contained protease inhibitors (mM): benzamidine HCl (2.5), e-amino-*n*-caproic acid (50), N-ethylmaleimide (0.5), phenylmethylsufonyl fluoride (0.3) and with pH adjusted to 7.4. The collagen matrices were thoroughly rinsed, lyophilized and stored at −70°C until use.

2.2 PVPA adsorption

Adsorption experiments were performed by mixing 50 mg of demineralized collagen with 1 mL of PVPA-containing solution for 1 min, 5 min or 1 h. Twelve PVPA (Mw 24,000, Sigma-Aldrich, St. Louis, MO, USA) solutions were prepared (0 to 20,000 μg/mL, based on serial dilutions) in 4 media: deionized water, 0.3 M EDC (pH 5.5; ThermoScientific Pierce, Rockford, IL, USA), 0.3 M EDC/0.06 M NHS (ThermoScientific Pierce) or 0.3 M EDC/0.3 M Im (Sigma-Aldrich). For the EDC-NHS protocol, NHS was added to the EDC and the pH adjusted to 5.5 with 0.1 M MES buffer. For the EDC-Im protocol, the Im solution was buffered to pH 5.5 with 0.1 N HCl prior to the addition of EDC. As PVPA adsorption and collagen cross-linking were conducted simultaneously, the EDC-Im protocol was used to validate our assumption that PVPA retention within collagen was not caused by direct cross-linking between PVPA and collagen, which should result in additional increase in the amount of immobilized PVPA.

After gentle tumbling at 37°C for the designated time points, the mixtures were centrifuged to retrieve the supernatant. The concentration of free PVPA in each supernatant was deduced by measuring its phosphorous content [29], using KH_2PO_4 as a phosphorus standard. Ammonium molybdate was incubated with the supernatant at 37°C for 2 h to produce a phosphomolybdate colored complex that was analyzed at 820 nm with a plate reader (Synergy HT, BioTek Instruments, Winooski, VT, USA). The amount of free PVPA (F) in the supernatant was calculated using a linear regression equation derived from known PVPA concentrations. The amount of immobilized PVPA was calculated by subtracting F from the initial amount of PVPA. Adsorption isotherms were plotted based on the relationship between PVPA adsorbed per unit mass of dried collagen (mg/g) and the PVPA concentration at equilibrium. Measurements were performed in triplicate.

2.3 PVPA desorption

Desorption of electrostatically bound PVPA was conducted using three salt concentrations: deionized water (i.e. 0 mM NaCl), 130 mM NaCl and 500 mM NaCl [30]. For each salt concentration, the twelve PVPA concentrations prepared with four media (i.e. deionized water, EDC only, EDC-NHS and EDC-Im) were first allowed to adsorb on demineralized collagen matrices for the optimal time period determined from the previous binding experiments. Thereafter, the PVPA-immobilized collagen matrices were briefly rinsed with deionized water and re-suspended in 1 mL of the respective desorbent at 37°C under mild agitation for 24 h. The supernatant was collected to determine the amount of PVPA desorbed by analysis of the phosphorus content [29]. Based on these data, PVPA solutions with the optimal EDC cross-linking method was selected for the subsequent parts of the experiments.

2.4 Statistical analyses

Non-linear regression was used to model the relationship between PVPA concentration and PVPA adsorption or PVPA that remained after immersion in the desorbents. Simultaneous tests of linear contrasts were used to compare model coefficients among groups. A Bonferroni adjustment was used to control the overall error rate for appropriately defined “families” of tests. The maximum PVPA uptake (B_{max}) was estimated based on the fitted curve and the interpolation method was used to estimate the concentration $K_{½}$ that would yield an uptake of $B_{max}/2$. This facilitates comparisons of the concentration of PVPA required to half-saturate the collagen matrix within the confines of the parameter being investigated. For each analysis

designed to test the three respective null hypotheses, the approximate 95% confidence interval for $K_{½}$ was used to derive an approximate standard error for $K_{½}$. The Wald test with a Bonferroni adjustment was used to compare $K_{½}$ values across treatment groups using these approximate standard errors. Two-tailed tests with a significance level of 0.05 were used for all statistical comparisons, except where the Bonferroni adjustment was applied.

Complementary Scatchard plots of the adsorption/desorption data were also generated by plotting the amount of bound PVPA to the free PVPA concentration as the ordinate and the amount of bound PVPA as the abscissa. These plots were used to determine if PVPA retention was characterized by a linear (one retention mode) or a curvilinear relation (heterogeneous retention). For the adsorption data, the tangent of each regression line/curve at its intersection with the ordinate was used to approximate the optimal PVPA concentration for "high affinity" retention.

2.5 Fourier transform-infrared spectroscopy (FT-IR)

A Nicolet 6700 FT-IR spectrophotometer (Thermo Scientific Inc., Waltham, MA, USA) with a diamond attenuated total reflection (ATR) setup was used to collect FT-IR spectra from the fibrous collagen matrices before (control) and after exposure to PVPA-cross-linking solutions with the optimal time period (i.e. 1 min, 5 min or 1 h) determined from the results of the binding experiments. The PVPA was applied to collagen matrices in the absence or presence of the most appropriate collagen cross-linking medium (i.e. EDC only, EDC/NHS, EDC/Im) derived from the results of the binding experiments. After cross-linking, the fibrous collagen matrices were rinsed three times with deionized water to remove excess PVPA and EDC and blot-dried with lint-free gauzes. Infrared spectra were collected between 675–4000 cm^{-1} at 4 cm^{-1} resolution using 32 scans.

2.6 Mineralization of reconstituted collagen

2.6.1 Self-assembly of collagen fibrils—A single-layer collagen mineralization model [31] was employed for rapid screening of the extent of intrafibrillar mineralization. Lyophilized type I collagen powder derived from calf skin (Sigma-Aldrich) was dissolved overnight in acetic acid containing phenol red at 4°C to obtain a 2 mg/mL collagen stock solution. Eighty μL droplets of the collagen solution were placed on an inert polyethylene substrate in a humidity chamber and a formvar- and carbon-coated Ni TEM grid (Electron Microscopy Sciences, Hatfield, PA, USA) was placed on top of each droplet. After neutralizing with ammonia, the collagen solution was left to gel by incubation at 37 °C. Confirmation of self-assembly of the collagen fibrils was performed by negative staining of randomly selected grids with 1% uranyl acetate followed by transmission electron microscopy (TEM; JEM-1230, JEOL, Tokyo, Japan) at 110 kV.

2.6.2 Mineralization of the PVPA-immobilized collagen fibrils—Seven PVPA concentrations were used for this part of the study: 0 (control), 200, 500, 1,000, 2,000, 4,000 and 8,000 μg/mL. Collagen cross-linking was performed using 0.3 M EDC only. Solutions with different PVPA concentrations were adjusted to pH 5. After adding EDC, the pH of the different solutions varied between 5.5–5.8. Collagen-coated grids were floated upside down in PVPA and EDC-containing solutions for 5 min. Thereafter, the grids were floated on a drop of 0.5 M NaCl for 5 min, dipped in and out of deionized water to remove electrostatically bound and unbound PVPA and air-dried. A calcium and hydroxyl ion-releasing composite composed of a light-polymerizable hydrophilic resin, set Portland cement powder (Lehigh Cement Company, Allentown, Pennsylvania, USA) and silanized colloidal silica (OX-50; Bisco, Inc., Schaumburg, IL, USA) was used for biomimetic mineralization of reconstituted collagen fibrils [31]. The Portland cement-based composite is capable of sustained release of Ca and OH ions, creating a medium with pH > 9.25 that is necessary for transformation of amorphous calcium

phosphate into apatite instead of octacalcium phosphate [32]. Resin disks of 6.0 ± 0.1 mm in diameter and 0.8 ± 0.02 mm thick were prepared by polymerization with a light-curing unit.

For each nanoscopic mineralization assembly, one 30 μL drop of simulated body fluid (SBF) containing 500 μg/mL polyacrylic acid (PAA, Mw 1,800; Sigma-Aldrich) was placed on top of a composite disk. The SBF was prepared by dissolving 136.8 mM NaCl, 4.2 mM $NaHCO_3$, 3.0 mM KCl, 1.0 mM $K_2HPO_4{\cdot}3H_2O$, 1.5 mM $MgCl_2{\cdot}6H_2O$, 2.5 mM $CaCl_2$ and 0.5 mM Na_2SO_4 in deionized water [33] containing 3.08 mM sodium azide to prevent bacterial growth. A TEM grid containing the PVPA cross-linked reconstituted collagen fibrils was then floated on top of the droplet and sealed inside the humidity chamber. The grids were incubated for 4 and 24 h in the humidity chamber at 37°C. After retrieval, each grid was dipped in and out of deionized water to remove loose precipitates and examined with TEM examination without further staining.

3. Results

3.1 PVPA adsorption and desorption

Figure 1A represents the adsorption isotherms obtained from the binding of PVPA to demineralized collagen matrices after 1 min, 5 min and 1 h, in the absence of EDC. The amount of sorbed PVPA increased with the time of contact with the collagen matrices, although most of the PVPA was adsorbed within the first 5 min. For the three time points investigated, no equilibrium binding could be established up to a PVPA concentration of 20,000 μg/mL. Quadratic polynomial models provided an excellent fit for the relationship between PVPA concentration and bound PVPA at 1 min, 5 min and 1 h, with highly significant omnibus F-tests ($p < 0.0001$) and large adjusted R^2 values ($R^2 > 0.998$) for each model. Simultaneous tests of linear contrasts with a Bonferroni-adjusted significance level of 0.05/3 = 0.0167 comparing the coefficients of the three models yielded a significant difference only in the linear term between the quadratic model fit to 1 min and the quadratic model fit to 1 h [$F(1, 16) = 10.75$, p = 0.005]. Table I contains the details of the estimation of $K_{½}$ for all three time points. The $K_{½}$ for 1 min differed significantly from the $K_{½}$ for 1 h ($z = 2.57$, $p = 0.010$). No other comparisons of $K_{½}$ values between groups were statistically significant at the Bonferroni-adjusted level of 0.0167. Similar trends were also obtained for the effect of time on PVPA sorption when cross-linking of the collagen matrices was mediated with EDC (i.e. EDC only, EDC/NHS, and EDC/Im; not shown). Linear Scatchard plots (Figure 1B) were obtained based on the data presented in Figure 1A.

As there was no difference in the amount of PVPA that interacted with the collagen matrices after 5 min versus 1 h of PVPA application, the 5 min time point was chosen for all subsequent experiments. Figure 2A represents the adsorption isotherms and 500 mM NaCl desorption isotherms for different PVPA concentrations after demineralized collagen matrices were cross-linked using EDC only, EDC/NHS or EDC/Im. Quadratic models provided excellent fits for the relationship between PVPA concentration and bound PVPA for the three adsorption isotherms and the three desorption isotherms. The omnibus F-tests were all highly significant ($p < 0.0001$) and adjusted R^2 values were > 0.996 for all six models. There were no significant differences among the three adsorption curves in terms of either the linear [omnibus $F(2, 21) = 0.63$, $p = 0.541$] or quadratic terms [omnibus $F(2, 21) = 1.00$, $p = 0.383$]. However, the omnibus F test showed a significant difference among the desorption curves in both the linear [$F(2, 21) = 11.08$, $p < 0.001$] and quadratic terms [$F(2, 21) = 5.36$, p = 0.013]. Simultaneous tests of linear contrasts with a Bonferroni-adjusted significance level of 0.05/3 = 0.0167 comparing the coefficients of the three desorption models yielded significant differences in the linear term when comparing the EDC only model with the EDC/NHS model [$F(1,14) = 15.93$, $p = 0.013$]. There were significant differences in the linear [$F(1,14) = 12.44$, $p = 0.003$] and quadratic [$F(1,14) = 9.22$, $p = 0.009$] terms when comparing the EDC/NHS model with the

EDC/Im model. Table II contains the details of the estimation of $K_{½}$ for the three adsorption and the three desorption models. For the adsorption models, there were differences in the $K_{½}$ values when comparing the EDC/Im group with the EDC only group ($z = 5.04$, $p < 0.001$) and the EDC/NHS group ($z = 2.86$, $p = 0.004$) using the Bonferroni-adjusted significance level of 0.0167. For the desorption models, the $K_{½}$ values for all three groups were significantly different from each other: EDC only *vs* EDC/NHS ($z = 3.84$, $p < 0.001$), EDC only *vs* EDC/Im ($z = 0.012$, $p < 0.001$), and EDC/NHS *vs* EDC/Im ($z = 6.04$, $p < 0.001$).

Figure 2B is the corresponding Scatchard plot of Fig. 2A. Unlike PVPA binding in the absence of EDC (Fig. 1A), transformation of the adsorption data yielded curvilinear Scatchard plots that are indicative of the presence of heterogeneous retention sites for each of the three EDC cross-linking methods. Following desorption in 500 mM NaCl, linear Scatchard plots were obtained from the transformed desorption data, which is indicative of a single retention mode.

As the desorption results indicated that cross-linking with EDC only yielded the best ligand retention characteristics, this cross-linking protocol was employed for the rest of the study. Figure 3 represents the effects of desorption salt concentration on PVPA-collagen interaction in the absence of EDC, and after PVPA was immobilized by cross-linking collagen with EDC only. For the interactions between collagen and PVPA applied in the absence of EDC (Fig. 3A), quadratic models provided an excellent fit for the relationships between PVPA concentration and bound PVPA at 5 min and between PVPA concentration and 24 h water desorption (i.e. 0 mM NaCl), with highly significant omnibus F-tests ($p < 0.0001$) and large adjusted R^2 values ($R^2 > 0.982$) for both models. Simultaneous tests of linear contrasts comparing the coefficients of the two quadratic models yielded a significant difference in the quadratic term [$F(1, 16) = 25.09$, $p < 0.001$]. Table III (upper part) contains the details of the estimation of $K_{½}$ for the two groups; the respective $K_{½}$ values for the two groups differed significantly ($z = 12.20$, $p < 0.001$). Complete desorption of the PVPA occurred after the application of 130 mM or 500 mM NaCl for 24 h.

For the interactions between collagen and PVPA applied with the use of EDC only (Fig. 3B), quadratic models provided an excellent fit for the relationship between PVPA concentration and bound PVPA, with highly significant omnibus F-tests ($p < 0.0001$) and large adjusted R^2 values ($R^2 > 0.997$) for all four models. Simultaneous tests of linear contrasts with a Bonferroni-adjusted significance level of 0.05/6 = 0.0083 comparing the coefficients of the four models yielded significant differences in the linear term when comparing the quadratic model for 5 min cross-linking with EDC only and the models for the desorption of PVPA by 130 mM NaCl [$F(1, 14) = 11.09$, $p = 0.005$] and the desorption of PVPA by 500 mM NaCl [$F(1, 14) = 29.58$, $p < 0.001$]. In addition, the quadratic model for 24 h desorption by water differed from the model for desorption by 500 mM NaCl in the linear term [$F(1,14) = 34.14$, $p < 0.001$]. Table III (lower part) contains the details of the estimation of $K_{½}$ for the four models. In terms of the Bonferroni-adjusted comparisons of the $K_{½}$ values across the four models, the $K_{½}$ values differed significantly between the 5 min cross-linking with EDC group and the 24 h desorption by water group ($z = 3.32$, $p < 0.001$) and the desorption by 500 mM NaCl group ($z = 3.78$, $p < 0.001$).

Figure 3C contains the corresponding Scatchard plots of the transformed adsorption data presented in Fig. 3B. A curvilinear plot was evident when PVPA was immobilized by EDC cross-linked collagen. A similar curvilinear Scatchard plot was also observed when desorption was conducted in water (i.e. 0 mM NaCl). Conversely, linear Scatchard plots were obtained with increasing ionic strength of the desorbent.

3.2 FT-IR spectroscopy

Figure 4 represents the IR spectra generated from demineralized collagen matrices before and after a 5-min period of immobilizing 500 μg/mL PVPA to the EDC cross-linked collagen matrix. Before treatment, the collagen matrix revealed characteristic collagen-related bands amide I, II and III at 1200–1700 cm^{-1} [34]. The amide A and B bands were obscured by the broad water region (2500–3700 cm^{-1}) present in the hydrated collagen [35]. Similar spectra were obtained after the immobilization of PVPA with the other two EDC cross-linking protocols. In particular, no new peaks were observed in the phosphate fingerprint region between 800–1500 cm^{-1} [36].

3.3 Mineralization of reconstituted collagen

Figure 5A is an image of stained reconstituted collagen fibrils prior to mineralization. Cross banding could be identified from fibrils that were wider than 50 nm in diameter. Unstained images of collagen fibrils retrieved after 4 h of incubation in the mineralization medium showed that they were not yet mineralized. Electron-dense mineral nanoprecursor aggregates could be seen along the periphery of the fibrils (Fig. 5B). For those fibrils in which PVPA was immobilized by EDC cross-linking, nanoprecursors were attached to the fibril surface in an ordered manner that roughly corresponded with the periodicity seen in stained fibrils (Fig. 5C). Those nanoprecursors failed to show diffraction rings when examined by selected area electron diffraction (SAED) that is indicative of their amorphous nature. They exhibited fluidity by coalescing to produce continuous phases (Fig. 5D).

The effect of PVPA concentration on the extent of collagen mineralization in grids retrieved after 24 h of incubation in the mineralization medium is illustrated by the low magnification unstained images in Figure 6. No mineralization could be seen when PVPA was absent (control, Fig. 6A). Mineralization was sparse in collagen fibrils that had been cross-linked with EDC to immobilize 4,000 or 8,000 μg/mL PVPA (Fig. 6B). A moderate extent of mineralization could be seen in collagen fibrils that had been cross-linked with EDC to immobilize 200 or 2,000 μg/mL PVPA (Fig. 6C). Heavy mineralization was observed in collagen fibrils that had been cross-linked with EDC to immobilize 500 or 1,000 μg/mL PVPA (Fig. 6D).

Unstained images of 24 h-mineralized collagen fibrils that had been cross-linked with EDC to immobilize 500 and 1,000 μg/mL PVPA are shown in Figure 7. Although no staining was employed, mineralized fibrils with immobilized PVPA exhibited a hierarchical order of mineral deposition as manifested by the recapitulation of their banding characteristics (Fig. 7A). However, SAED of these fibrils indicated that the mineralized phase within the fibrils were amorphous in nature. Extrafibrillar mineral deposits were commonly observed (Fig. 7A) and appeared to be crystalline aggregates of nanocrystals with roughly hexagonal crystalline planes that were 5–15 nm in length along their C-axis (Fig. 7B). Although cross-banding was not evident due to the three-dimensional method of observation, the fibrils exhibited periodic elevations along their external surfaces (Fig. 7C). At high magnification, nanocrystals were arranged longitudinally along the more heavily mineralized fibrils. The nanocrystals were confirmed by SAED to be apatite (Fig. 7D).

4. Discussion

As there was significant difference in the amount of PVPA immobilized within the collagen matrices following 1 min and 1 h of PVPA-EDC application, the first null hypothesis has to be rejected. As no significant difference was observed between 5 min and 1 h of PVPA-EDC application, the former time point was selected for subsequent experiments. As the stability of PVPA immobilization was improved after the collagen matrices were cross-linked with EDC, the second null hypothesis was rejected and collagen cross-linking was adopted for subsequent

mineralization experiments. As there was no additional improvement in PVPA retention when N-hydroxysuccinimide or imidazole was employed with EDC for cross-linking demineralized collagen, the third null hypothesis has to be accepted and EDC alone was adopted as the collagen cross-linking protocol.

The use of PVPA concentrations up to 20,000 μg/mL did not achieve maximum binding to demineralized collagen matrices (Fig. 1). This may be due to increase in surface area and binding capacity as the dentin was reduced to a fine powder. When 500 mM NaCl was used as a desorbent, the PVPA molecules were completely eluted from the demineralized collagen in the absence of collagen cross-linking. This finding corresponds well with the single retention mode delineated by the linear Scatchard plots [37,38] in Fig. 1B. Taken together, the results confirm that binding of PVPA to collagen molecules is electrostatic in nature. Desorption of electrostatically bound PVPA by the anions present in the SBF is likely to result in suboptimal mineralization within the collagen fibrils. Although dentin collagen is more highly cross-linked than bone collagen, additional cross-linking may be introduced using various agents [39]. The curvilinear Scatchard plots obtained after collagen was cross-linked with EDC or EDC-NHS are indicative of the presence of a heterogeneous family of PVPA retention mechanisms with different degrees of affinity to the cross-linked collagen (Fig. 2B). These mechanisms may include electrostatic binding, size exclusion by the cross-linked collagen or covalent cross-linking. The observation that there was no increase in the amount of immobilized PVPA after the use of the EDC-Im cross-linking protocol argues against the existence of covalent cross-linking between PVPA and collagen molecules (Fig. 2A). The absence of new peaks in FT-IR spectroscopy (Fig. 4) further substantiated the absence of covalent cross-links between PVPA and collagen. This leaves behind electrostatic binding and size exclusion by the cross-linked collagen as the potential retention mechanisms for PVPA after it was applied with simultaneous collagen cross-linking to the collagen matrices.

All electrostatically bound PVPA molecules were displaced after desorption in 500 mM NaCl. The initial curvilinear Scatchard plots [37,38] associated with PVPA desorption in deionized water became linear Scatchard plots with increases in ionic concentration of the desorbent (Fig. 3C). As the ionic strength of water is much weaker than the NaCl solutions, it was incapable of displacing all the electrostatically-bound PVPA from a collagen matrix. This accounts for the curvilinear nature of the Scatchard plots after water desorption. With respect to the linear Scatchard plots observed after 500 mM NaCl desorption, this high affinity “irreversible” binding mode should logically be interpreted as entrapment of the PVPA molecules within the intrafibrillar water compartments of collagen [40] and not actual covalent cross-linking of PVPA to collagen, based on the EDC-Im and FT-IR results. Type I collagen exhibits size exclusion characteristics which limit the size of molecules that can penetrate its internal water compartments. Molecules smaller than 40 kDa are completely excluded while those smaller than 6 kDa can diffuse into all water compartments of a collagen fibril [27]. The average molecular size of PVPA reported by the manufacturer (24 kDa) is really a mixture of PVPA polymers that include some that are smaller and larger than 24 kDa [41]. The smaller molecules can enter the water compartments of collagen. By cross-linking collagen with EDC, a zero-length cross-linking agent, we can increase the sieving properties of collagen and trap PVPA within collagen.

Although the adsorption isotherms generated valuable information on the binding characteristics of PVPA to collagen, they provided limited information on whether the equilibrium binding concentration (*Bmax*) represents the best concentration for mineralization of collagen fibrils. It is known that only a very small amount of phosphoproteins is required for regulating mineral deposition during osteogenesis and dentinogenesis [15]. Thus, in the subsequent part of the study, the approximated PVPA concentration range derived from the tangent of the high affinity part of the curvilinear Scatchard plot was screened using the single-

layer collagen mineralization model [31] prior to the translation of the PVPA retention protocol for practical applications.

Intrafibrillar mineralization contributes significantly to the biomechanical properties of mineralized collagenous tissues [42]. In natural mineralization, binding of matrix phosphoproteins to collagen at specific sites such as the gap zones and pores of the fibrillar assembly is necessary for initiation of intrafibrillar mineralization. Previous studies that employed phosphoprotein analogs for mineralization of collagen fibrils only resulted in the deposition of large needle-shaped crystals or large spherical calcium phosphate clusters around the phosphorylated collagen fibrils [21,43–45]. In those studies, there was no sequestering mechanism such as the use of polyaspartic acid or PAA for stabilizing the amorphous calcium precursors in a nanoscale [7,8,46]. As the apatite clusters created were too large to fit into the body of the collagen fibrils [43–45], no intrafibrillar minerals and banding patterns could be discerned within the fibrils. Over the last decade, a growing body of evidence emerges indicating that large single-crystal biominerals are not formed from their ion constituents but from amorphous precursor phases [47]. Sequestration of liquid-like amorphous mineral nanoprecursors [48] and self-assembly of nanocrystals into polymer-stabilized mesocrystalline phases [49] are processes that contribute to the particle-mediated mechanism of biomineralization [18]. In the present study, this mechanism has been adopted with the use of two biomimetic analogs to achieve mineralize reconstituted type I collagen fibrils that were devoid of matrix proteins as well as apatite seed crystallites. The PVPA biomimetic molecules probably simulate the calcium phosphate binding sites of matrix phosphoproteins and act as templates for recruiting PAA-stabilized ACP nanoprecursors to the internal water compartments of the collagen fibrils. Consistent with previous findings, we have been able to observe electron-dense, nanoprecursors congregating around the periphery of collagen fibrils at an early stage of mineralization (Figs 5B, 5C). The larger precursors appear to have formed by the coalescence of multiple smaller nanoprecursors, indirectly substantiating the fluidity of these amorphous droplets. As these fluidic droplets are mostly smaller than 50 nm in diameter, they are capable of infiltrating collagen fibrils to fill the gap zones between the collagen molecules and spaces between the microfibrils. These observations confirm the role played by amorphous nanoprecursor particles in biomimetic mineralization, and advance our knowledge on how biomineralization may be biomimetically recapitulated based on the non-classical crystallization pathway [18,19].

It is interesting that immobilization of 500 and 1000 μg/mL PVPA within the reconstituted collagen showed more heavily mineralization when compared to immobilization of 200 and 2000 μg/mL PVPA (Figs. 6C, 6D). We speculate that at low PVPA concentrations (< 500 μg/mL), the amount of PVPA may not be optimal to induce heavy mineralization of the collagen fibrils. Conversely, at high PVPA concentrations (>1,000 μg/mL), the analog may act as an inhibitor instead of a promoter of biomineralization [50]. This illustrates the use of the TEM grid model for expediting the examination of the optimal concentration range of biomimetic analogs.

We utilized a zero-length cross-linking agent instead of non-zero-length cross-linking agents such as glutaraldehyde to augment the size exclusion effect by not introducing additional extrinsic spacers between the cross-linked collagen molecules. Immobilization of PVPA molecules via this size exclusion mechanism enables them to function as templates for nucleation and growth of apatites within the collagen matrices. This provided a plausible explanation for the observation of mineralized collagen fibrils with cross-banding characteristic in PVPA-retained collagen (Fig. 7A). It is noteworthy that the nanocrystals shown in Fig. 7D appear to be much smaller than the apatite platelets deposited in natural mineralized collagen fibrils. Larger apatite platelets with more definitive SAED apatite ring patterns were observed from highly electron-dense, banded mineralized fibrils after 72 h of

mineralization with the same model (unpublished results). Mesocrystals are kinetically metastable intermediates that fuse to produce a single crystal [49]. We speculate that the intrafibrillar nanocrystals represent mesocrystalline phases that eventually fuse to produce apatite platelets [51]. This hypothesis has to be substantiated in future work.

The present study provides a technique for removing a concept-proven templating analog of matrix phosphoproteins from the mineralization medium by entrapping it within a collagen matrix based on a size exclusion mechanism. The discovery that cross-linking may be performed within a short time period (i.e. 5 min) opens new vistas for *in-situ* applications of the proposed biomimetic mineralization strategy. Understanding the basic processes in intrafibrillar mineralization of reconstituted collagen fibrils creates new opportunities for the design of tissue engineering materials for hard tissue repair and regeneration.

Acknowledgments

This study was supported by Grant R21 DE019213-01 from the National Institute of Dental and Craniofacial Research (PI. Franklin R. Tay). The work was performed in the Medical College of Georgia. We thank Michelle Barnes for secretarial support. Dr. Lisha Gu was supported by a scholarship from the Chinese Scholarship Council. Data derived from this study was submitted to Guanghua School of Stomatology, Sun Yat-sen University in partial fulfilment of Dr. Gu's PhD requirements in China.

References

1. Glimcher MJ. Mechanism of calcification: role of collagen fibrils and collagen-phosphoprotein complexes in vitro and in vivo. Anat Rec 1989;224:139–153. [PubMed: 2672881]
2. Tao J, Pan H, Zeng Y, Xu X, Tang R. Roles of amorphous calcium phosphate and biological additives in the assembly of hydroxyapatite nanoparticles. J Phys Chem B 2007;111:13410–13418. [PubMed: 17979266]
3. Veis, A. The role of acidic proteins in biological mineralization. In: Everett, DH.; Vincent, G., editors. Ions in Macromolecular and Biological Systems. Bristol, United Kingdom: Scientechnia; 1978. p. 259-267.
4. Sfeir, C.; Campbell, P.; Jadlowied, JA.; Kumta, P. Method of inducing biomineralization method of inducing bone regeneration and methods related thereof. United States Patent Application. 20070087959. Apr 19. 2007
5. Goldberg HA, Warner KJ, Li MC, Hunter GK. Binding of bone sialoprotein, osteopontin and synthetic polypeptides to hydroxyapatite. Connect Tissue Res 2001;42:25–37. [PubMed: 11696986]
6. Niederberger M, Cölfen H. Oriented attachment and mesocrystals: non-classical crystallization mechanisms based on nanoparticle assembly. Phys Chem Chem Phys 2006;8:3271–3287. [PubMed: 16835675]
7. Tay FR, Pashley DH. Guided tissue remineralisation of partially demineralised human dentine. Biomaterials 2008;29:1127–1137. [PubMed: 18022228]
8. Tay FR, Pashley DH. Biomimetic remineralization of resin-bonded acid-etched dentin. J Dent Res 2009;88:719–724. [PubMed: 19734458]
9. Gower LB, Odom DJ. Deposition of calcium carbonate films by a polymer-induced liquid-precursor (PILP) process. J Crystal Growth 2000;210:719–734.
10. Song RQ, Cölfen H, Xu AW, Hartmann J, Antonietti M. Polyelectrolyte-directed nanoparticle aggregation: Systematic morphogenesis of calcium carbonate by nonclassical crystallization. ACS Nano. 2009 Jul 2; Epub ahead of print.
11. Olszta MJ, Odom DJ, Douglas EP, Gower LB. A new paradigm for biomineral formation: Mineralization via an amorphous liquid-phase precursor. Connect Tissue Res 2003;44:326–334. [PubMed: 12952217]
12. Landis WJ, Song MJ, Leith A, McEwen L, McEwen BF. Mineral and organic matrix interaction in normally calcifying tendon visualized in three dimensions by high-voltage electron microscopic tomography and graphic image reconstruction. J Struct Biol 1993;110:39–54. [PubMed: 8494671]

13. Mahamid J, Sharir A, Addadi L, Weiner S. Amorphous calcium phosphate is a major component of the forming fin bones of zebrafish: Indications for an amorphous precursor phase. Proc Natl Acad Sci U S A 2008;105:12748–12753. [PubMed: 18753619]
14. Pouget EM, Bomans PH, Goos JA, Frederik PM, de With G, Sommerdijk NA. The initial stages of template-controlled CaCO3 formation revealed by cryo-TEM. Science 2009;323:1455–1458. [PubMed: 19286549]
15. George A, Veis A. Phosphorylated proteins and control over apatite nucleation, crystal growth and inhibition. Chen Rev 2008;108:4670–4693.
16. Sampath TK, Reddi AH. Dissociative extraction and reconstitution of extracellular matrix components involved in local bone differentiation. Proc Natl Acad Sci U S A 1981;78:7599–7603. [PubMed: 6950401]
17. Endo A, Glimcher MJ. The effect of complexing phosphoproteins to decalcified collagen on in vitro calcification. Connect Tissue Res 1989;21:179–190. [PubMed: 2605942]
18. Xu AW, Ma YR, Cölfen H. Biomimetic mineralization. J Mater Chem 2007;17:415–449.
19. Meldrum FC, Cölfen H. Controlling mineral morphologies and structures in biological and synthetic systems. Chem Rev 2008;108:4332–4432. [PubMed: 19006397]
20. Linde A, Lussi A, Crenshaw MA. Mineral induction by immobilized polyanionic proteins. Calcif Tissue Int 1989;44:286–295. [PubMed: 2501010]
21. Saito T, Arsenault AL, Yamauchi M, Kuboki Y, Crenshaw MA. Mineral induction by immobilized phosphoproteins. Bone 1997;21:305–311. [PubMed: 9315333]
22. Komber H, Steinert V, Voit B. ^{1}H, ^{13}C and ^{31}P NMR study on poly(vinylphosphonic acid) and its dimethyl ester. Macromolecules 2008;41:2119–2125.
23. Rivas BL, Pereira E, Gallegos P, Homper D, Geckeler KE. Metal ion binding capacity of the water-soluble poly(vinyl phosphonic acid) for mono-, di-, and trivalent cations. J Appl Polym Sci 2004;92:2917–2922.
24. Grabarek Z, Gergely J. Zero-length crosslinking procedure with the use of active esters. Anal Biochem 1990;185:131–135. [PubMed: 2344038]
25. Staros JV, Wright RW, Swingle DM. Enhancement by N-hydroxysulfosuccinimide of water-soluble carbodiimide-mediated coupling reactions. Anal Biochem 1986;156:220–222. [PubMed: 3740412]
26. Pall GS, Codony-Servat C, Byrne J, Ritchie L, Hamilton A. Carbodiimide-mediated cross-linking of RNA to nylon membranes improves the detection of siRNA, miRNA and piRNA by northern blot. Nucleic Acids Res 2007;35:e60. [PubMed: 17405769]
27. Toroian D, Lim JE, Price PA. The size exclusion characteristics of type I collagen: implications for the role of noncollagenous bone constituents in mineralization. J Biol Chem 2007;282:22437–22447. [PubMed: 17562713]
28. Sampath TK, Reddi AH. Distribution of bone inductive proteins in mineralized and demineralized extracellular matrix. Biochem Biophys Res Commun 1984;119:949–954. [PubMed: 6712678]
29. Chen PS Jr, Toribara TY, Warner H. Microdetermination of phosphorus. Anal Chem 1956;28:1756–1758.
30. Singh MP, Lumpkin JA, Rosenblatt J. Effect of electrostatic interactions on polylysine release rates from collagen matrices and comparison with model predictions. J Control Release 1995;35:165–179.
31. Kim YK, Gu L-S, Bryan TE, Kim JR, Chen L, Liu Y, Yoon JC, Breschi L, Pashley DH, Tay FR. Mineralization of reconstituted collagen using polyvinylphosphonic acid/polyacrylic acid templating matrix protein analogues in the presence of calcium, phosphate and hydroxyl ions. Biomaterials 2010;31:6618–6627. [PubMed: 20621767]
32. Meyer JL, Eanes ED. A thermodynamic analysis of the secondary transition in the spontaneous precipitation of calcium phosphate. Calcif Tissue Res 1978;25:209–216. [PubMed: 30523]
33. Kokubo T, Kushitani H, Sakka S, Kitsugi T, Yamamuro T. Solutions able to reproduce in vivo surface-structure changes in bioactive glass-ceramic A-W. J Biomed Mater Res 1990;24:721–734. [PubMed: 2361964]
34. Chang MC, Tanaka J. FT-IR study for hydroxyapatite/collagen nanocomposite cross-linked by glutaraldehyde. Biomaterials 2002;23:4811–4818. [PubMed: 12361620]

35. Bachmann L, Baffa O, Zezell DM. Thermal degradation of dentin collagen evaluated with ESR, infrared and optical spectroscopy. Philos Mag 2007;87:1033–1042.
36. Ishii K, Yanase K, Suzuki S, Yamamoto M, Chihara K, Tabata Y, et al. Phosphorylation analysis using FT-IR and the application for an evaluation of biomaterials. J Jpn Soc Infrared Sci Technol 2004;14:44–50.
37. Scatchard G. The attraction of proteins for small molecules and ions. Ann N Y Acad Sci 1949;51:660–672.
38. Morin R, Kaplan D, Perez-Ramirez B. Bone morphogenetic protein-2 binds as multilayers to a collagen delivery matrix: an equilibrium thermodynamic analysis. Biomacromolecules 2006;7:131–138. [PubMed: 16398507]
39. Al-Ammar A, Drummond JL, Bedran-Russo AK. The use of collagen cross-linking agents to enhance dentin bond strength. J Biomed Mater Res B Appl Biomater 2009;91:419–24. [PubMed: 19507140]
40. Fullerton GD, Nes E, Amurao M, Rahal A, Krasnosselskaia L, Cameron I. An NMR method to characterize multiple water compartments on mammalian collagen. Cell Biol Int 2006;30:66–73. [PubMed: 16376582]
41. Stranberg C, Rosenauer C, Wegner G. Poly(vinyl phosphonic acid): Hydrodynamic properties and SEC-calibration in aqueous solution. Macromol Rapid Comm 2010;31:374–9.
42. Kinney JH, Habelitz S, Marshall SJ, Marshall GW. The importance of intrafibrillar mineralization of collagen on the mechanical properties of dentin. J Dent Res 2003;82:957–961. [PubMed: 14630894]
43. Bradt JH, Mertig M, Teresiak A, Pompe W. Biomimetic mineralization of collagen by combined fibril assembly and calcium phosphate formation. Chem Mater 1999;11:2694–2701.
44. Lickorish D, Ramshaw JA, Werkmeister JA, Glattauer V, Howlett CR. Collagen-hydroxyapatite composite prepared by biomimetic process. J Biomed Mater Res A 2004;68:19–27. [PubMed: 14661245]
45. Li X, Chang J. Preparation of bone-like apatite-collagen nanocomposites by a biomimetic process with phosphorylated collagen. J Biomed Mater Res A 2008;85:293–300. [PubMed: 17688292]
46. Deshpande AS, Beniash E. Bio-inspired synthesis of mineralized collagen fibrils. Cryst Growth Des 2008;8:3084–3090.
47. Politi Y, Arad T, Klein E, Weiner S, Addadi L. Sea urchin spine calcite forms via a transient amorphous calcium carbonate phase. Science 2004;306:1161–1164. [PubMed: 15539597]
48. Gower LB. Biomimetic model systems for investigating the amorphous precursor pathway and its role in biomineralization. Chem Rev 2008;108:4551–4627. [PubMed: 19006398]
49. Cölfen H, Mann S. Higher-order organization by mesoscale self-assembly and transformation of hybrid nanostructures. Angew Chem Int Ed 2003;42:2350–2365.
50. Boskey AL. Biomineralization: an overview. Connect Tissue Res 2003;44(Suppl 1):5–9. [PubMed: 12952166]
51. Zhang TH, Liu XY. How does a transient amorphous precursor template crystallization. J Am Chem Soc 2007;129:13520–13526. [PubMed: 17929918]

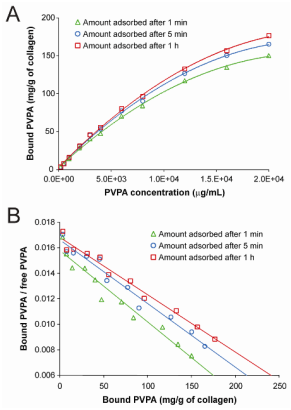

Fig. 1.

A. Adsorption isotherms showing the binding of different PVPA concentrations to demineralized collagen matrices in the absence of carbodiimde (EDC) at 1 min (open triangle), 5 min (open circle) and 1 h (open square) at 37°C. Each point represents the mean of triplicate assays. **B**. Linear Scatchard plots corresponding to the adsorption isotherms in Fig. 1A.

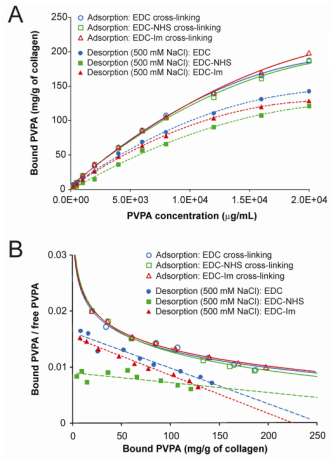

Fig. 2.

A. Adsorption isotherms (open designators) and desorption isotherms (solid designators) (500 mM NaCl) for different PVPA concentrations after they were immobilized to demineralized collagen matrices cross-linked with EDC only (circles), EDC/N-hydroxysuccinimide (NHS; squares) and EDC/imidazole (Im; triangles) at 37°C. Each point represents the mean of triplicate assays. **B**. Scatchard plots corresponding to the isotherms in Fig. 2A.

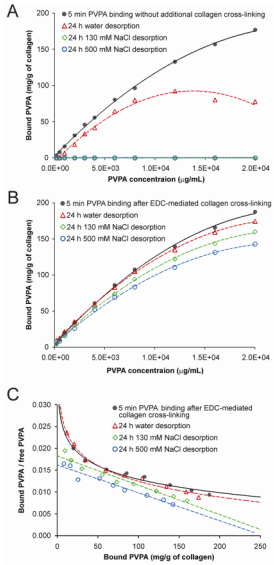

Fig. 3.

Desorption isotherms showing the effects of ionic concentration of the environment on desorption of PVPA from cross-linked collagen matrices. Each point represents the mean of triplicate assays. **A**. PVPA was applied for 5 min to the collagen matrices in the absence of EDC (black solid circles, solid trend line). Without being immobilized within the collagen, PVPA completely desorbed in the presence of 130 mM and 500 mM NaCl after 24 h and produced the same (zero) line-plot along the abscissa. **B**. Collagen was cross-linked with EDC only for 5 min (black solid circles, solid trend lines). For both cases, the desorption media were: i) deionized water (open triangles, dotted trend lines); ii) 130 mM NaCl (open rotated squares, dotted trend lines); and iii) 500 mM NaCl (open squares, dotted trend lines). **C.** Scatchard plots corresponding to the isotherms of EDC-cross-linked collagen matrices depicted in Fig. 3B, with similar group designators.

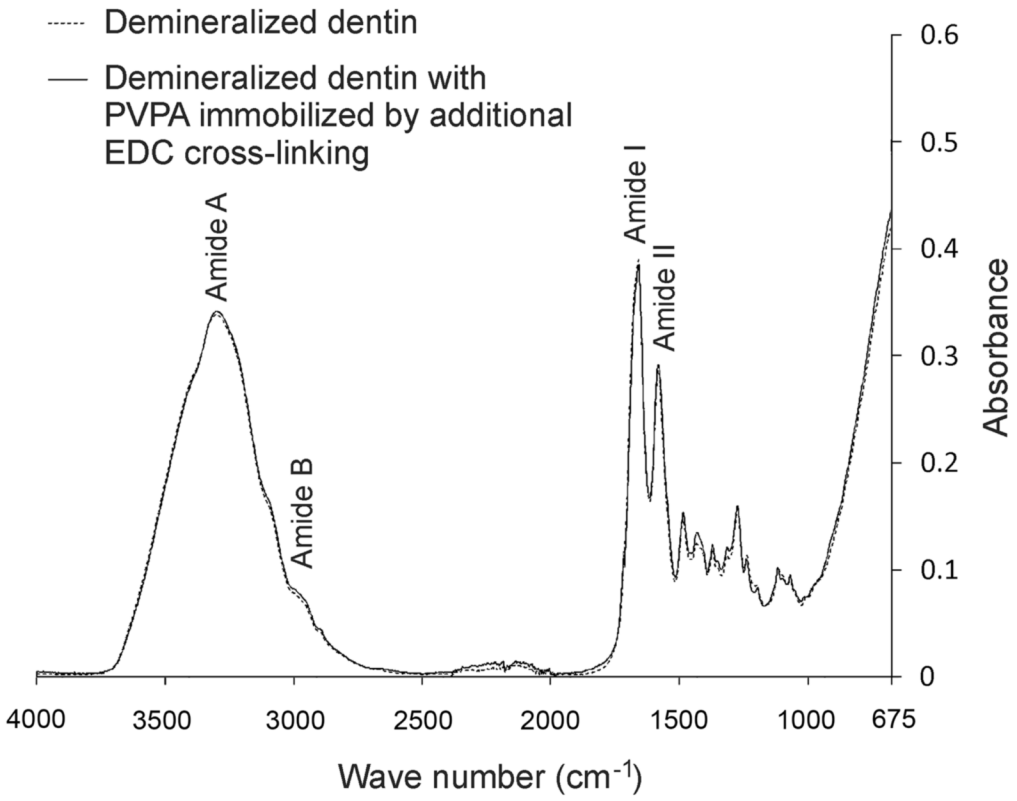

Fig. 4.

Infrared spectra of demineralized dentin collagen matrices before (dotted line) and after (solid line) cross-linking with EDC to immobilize PVPA. Similar results were obtained when EDC cross-linking of collagen was performed in the presence of N-hydroxysuccinimide and imidazole (not shown).

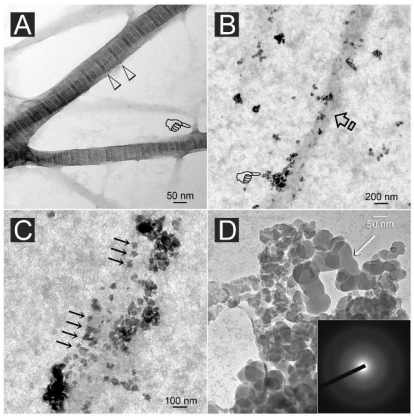

Fig. 5.

A. Stained image of reconstituted type I collagen showing an approximately 76 nm periodicity (open arrowheads) in fibrils that are larger than 50 nm in diameter. Branching of the fibrils could frequently be observed (pointer). **B**. Unstained, PVPA-immobilized collagen fibril (arrow) retrieved after 4 h of immersion in the mineralization medium (see text). Electron-dense nanospheres (pointer) aggregated along the periphery of the unmineralized fibril. **C**. Unstained image showing attachment of electron-dense nanospheres along an unmineralized fibril with a periodicity (arrows) that roughly corresponded with the D-period of a stained fibril. **D**. High magnification of the partially coalesced nanospheres (arrow) illustrating the fluidity of the nanoprecursor phase. Inset: Electron diffraction revealed a diffuse pattern characteristic of the amorphous nature of the initially formed minerals.

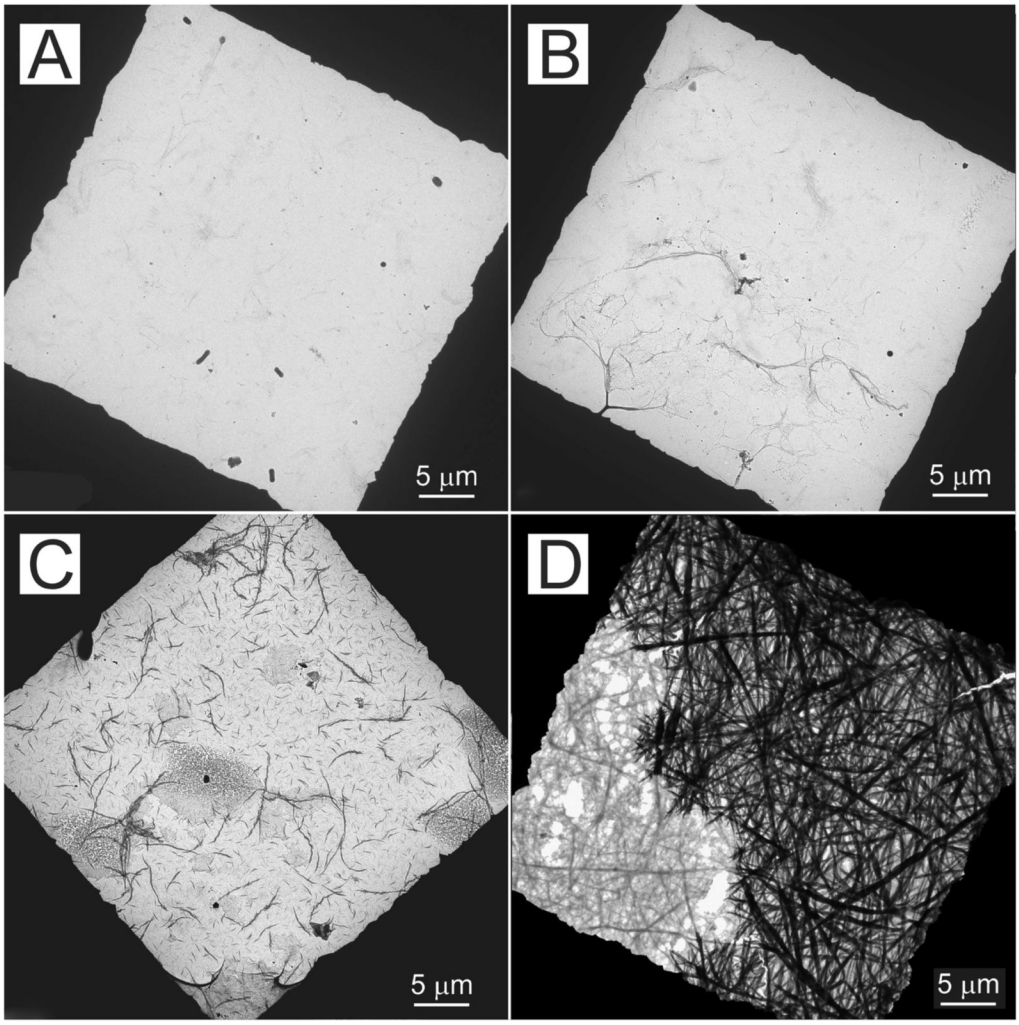

Fig. 6.

Unstained low magnification TEM images showing the extent of collagen fibril mineralization within one square frame of a 400-mesh formvar- and carbon-coated grid containing reconstituted type I collagen fibrils. The grids were all retrieved from the mineralization medium after 24 h. The black periphery represents the grid bars. **A**. No mineralization (PVPA absent). **B**. Sparse mineralization (collagen cross-linked with EDC to immobilize 4,000 or 8,000 μg/mL PVPA). **C**. Moderate mineralization (collagen cross-linked with EDC to immobilize 200 or 2,000 μg/mL PVPA). **D**. Dense mineralization (collagen cross-linked with EDC to immobilize 500 or 1,000 μg/mL PVPA).

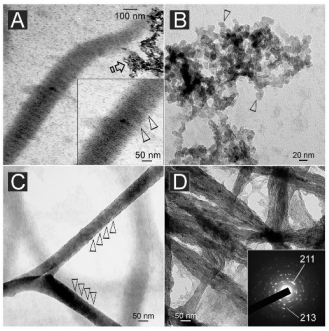

Fig. 7.

A. Unstained reconstituted collagen fibrils cross-linked with EDC to immobilize 500–1,000 μg/mL of PVPA within the fibrils and retrieved after incubation in the mineralization medium for 24 h. Electron-dense intrafibrillar minerals were deposited in a manner that revealed the periodicity of the fibrils (inset: between open arrowheads). **B**. Unstained image of the aggregates depicted by the open arrow in **A** revealed formation of angular nanocrystals with roughly hexagonal appearance (open arrowheads). **C**. Unstained, highly mineralized reconstituted collagen fibrils that were retrieved after 24 h. Elevations along the periphery of the mineralized fibril revealed a vague periodicity (open arrowheads). **D**. Unstained image of similar mineral fibrils showing the formation of electron-dense nanocrystals within the fibrils. Internal periodicity could not be identified due to the three-dimensional nature of the fibrils. Inset: concentric ring patterns with arc-shaped patterns in the (211) plane that are indicative of the formation of apatite with a regular orientation (i.e. parallel to the longitudinal axis of the collagen fibril).

Table I

Estimates of $K_{½}$ for PVPA binding in the absence of EDC at different time periods

PVPA-collagen interaction time	B_{max}	$B_{max}/2$	Estimate of $K_{½}$	95% CI ($K_{½}$)	Approx. S.E.
1 min	153.11	76.56	6845.76	6603.1–7092.4	122.33
5 min	170.05	85.02	6994.10	6710.18–7286.69	144.13
1 h	182.96	91.48	7282.80	7050.95–7522.87	117.98

Abbreviations: PVPA = polyvinylphosphonic acid; EDC = carbodiimide

Table II

Estimates of $K_{½}$ for adsorption and desorption after the use of three different EDC cross-linking protocols for immobilizing PVPA within the EDC-cross-linked collagen matrices

	Cross-linking Protocol	B_{max}	$B_{max}/2$	Estimate of $K_{½}$	95% CI ($K_{½}$)	Approx. S.E.
Adsorption	EDC only	192.04	96.02	7093.05	6825.44–7370.45	136.25
	EDC/NHS	193.72	96.86	7446.02	7006.28–7894.16	221.97
	EDC/Im	216.12	108.06	8289.98	7906.74–8683.97	194.31
Desorption	EDC only	144.45	72.22	6532.98	6272.24–6799.09	131.71
	EDC/NHS	125.70	62.85	7455.93	7062.41–7865.60	200.80
	EDC/Im	128.83	64.41	6134.97	5958.37–6306.35	86.99

Abbreviations: EDC = carbodiimide; NHS = N-hydroxysuccinimide; Im = imidazole

Acta Biomater. Author manuscript; available in PMC 2012 January 1.

Table III

Estimates of $K_{½}$ for PVPA adsorption and desorption (24 h) in the absence and presence of EDC

		Treatment	B_{max}	$B_{max}/2$	Estimate of $K_{½}$	95% CI ($K_{½}$)	Approx. S.E.
No EDC		Adsorption	182.96	91.48	7282.80	7050.95–7522.87	117.98
EDC only	Desorption	0 mM NaCl *	92.41	46.21	4315.28	3901.71–4752.19	212.62
		130 mM NaCl	NA	NA	NA	NA	NA
		500 mM NaCl	NA	NA	NA	NA	NA
		Adsorption	192.04	96.02	7093.05	6825.44–7370.45	136.25
		0 mM NaCl *	177.46	88.73	6586.92	6448.19–6720.97	68.19
		130 mM NaCl	162.11	81.05	6726.29	6496.37–6958.65	115.57
		500 mM NaCl	141.27	70.63	6379.76	6150.23–6671.59	130.34

*Deionized water